

Supporting Information

Degradable Semiconducting Oligomer Amphiphile for Ratiometric Photoacoustic Imaging of Hypochlorite

Chao Yin,^{†,‡,+,*} Xu Zhen,^{‡,+,*} Quli Fan,^{*,†} Wei Huang,^{†,§} and Kanyi Pu^{*,‡}

[†]Key Laboratory for Organic Electronics and Information Displays & Institute of
Advanced Materials (IAM), Jiangsu National Synergetic Innovation Center for
Advanced Materials (SICAM), Nanjing University of Posts & Telecommunications, 9
Wenyuan Road, Nanjing 210023, China

*E-mail: iamqlfan@njupt.edu.cn

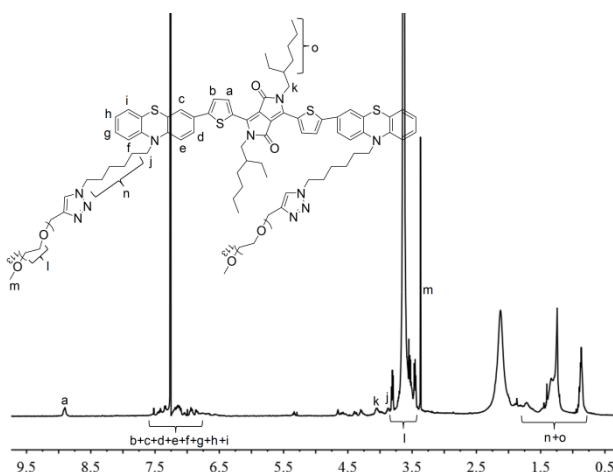
[‡]School of Chemical and Biomedical Engineering, Nanyang Technological
University, 70 Nanyang Drive, Singapore, 637457

*E-mail: kypu@ntu.edu.sg

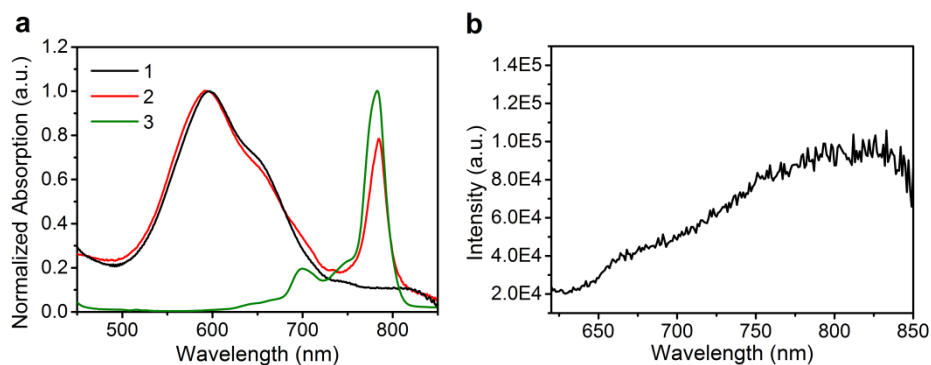
[§]Key Laboratory of Flexible Electronics (KLOFE) & Institute of Advanced Materials
(IAM), Jiangsu National Synergetic Innovation Center for Advanced Materials
(SICAM), Nanjing Tech University (NanjingTech), 30 South Puzhu Road, Nanjing
211816, China

⁺Both authors contributed equally to this work.

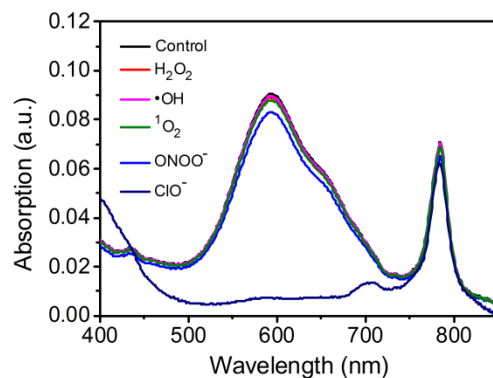
Supporting Figures



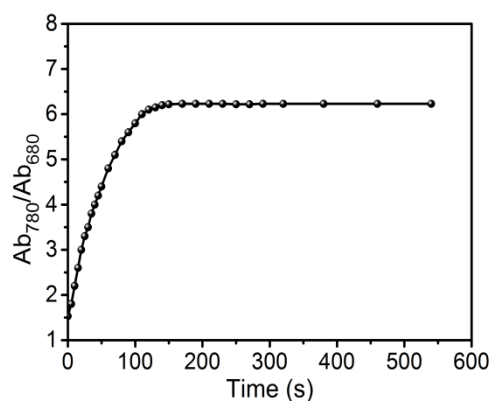
Supporting Figure S1. ^1H NMR spectrum of the SOA (compound 7). CDCl_3 was used as the solvent.



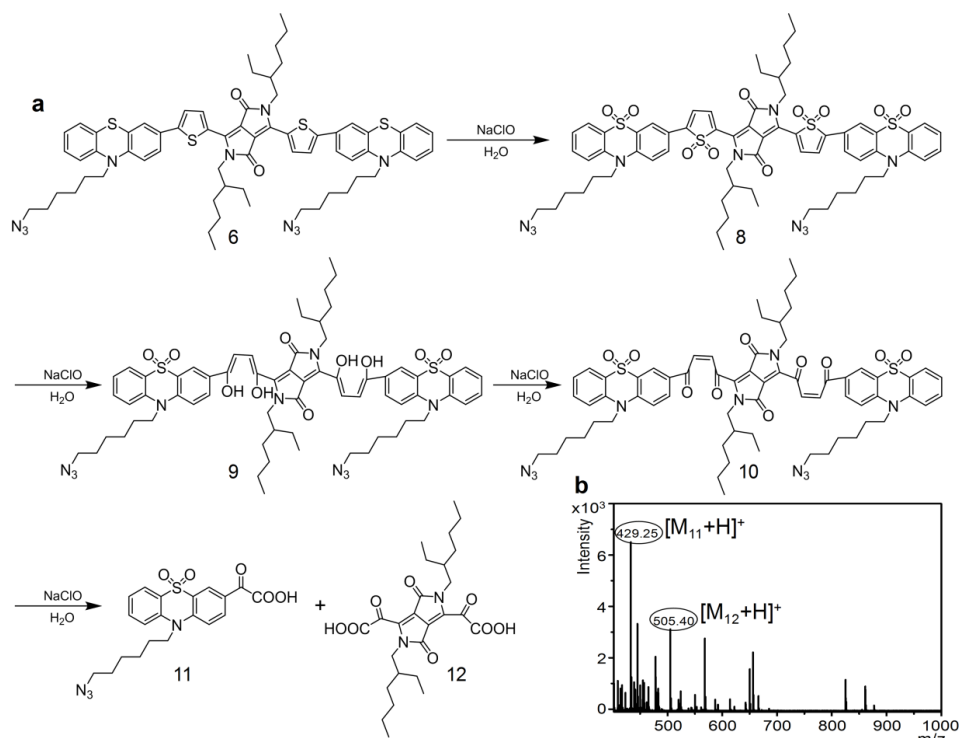
Supporting Figure S2. a) Normalized UV-Vis absorption spectra of the SOA (1), the nanoprobe (2), and PEG-*b*-PPG-*b*-PEG encapsulated NIR775 nanoparticles (3) in 1×PBS (pH = 7.4). b) Fluorescence spectrum of the SOA (compound 7) in 1×PBS (pH = 7.4) upon excitation at 600 nm.



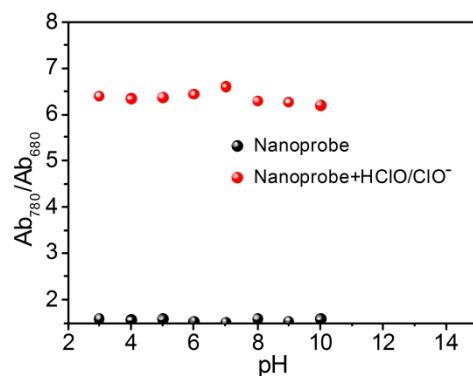
Supporting Figure S3. Representative UV-Vis spectra of the nanoprobe ($30 \mu\text{g mL}^{-1}$) in the absence (black) and presence (red = hydrogen peroxide, magenta = hydroxyl radicals, olive = singlet oxygen, blue = peroxynitrite, navy = hypochlorite) of ROS ($11 \mu\text{M}$).



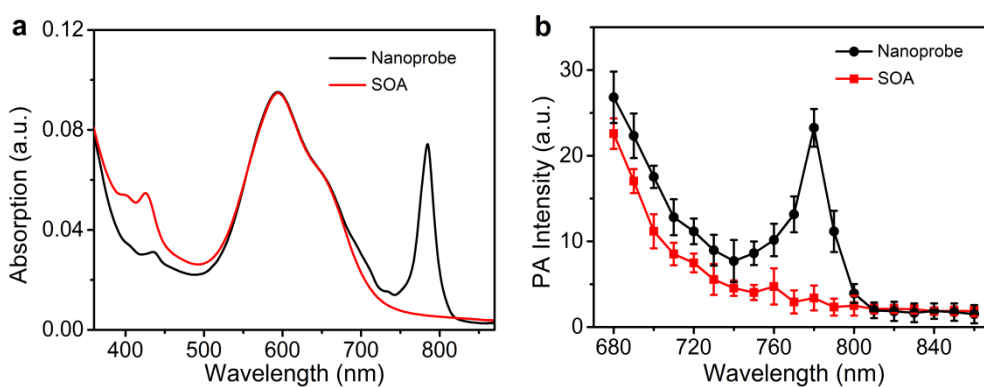
Supporting Figure S4. The ratiometric absorption ($\text{Ab}_{780}/\text{Ab}_{680}$) of the nanoprobe ($30 \mu\text{g mL}^{-1}$) as a function of time in the presence of ClO^- ($11 \mu\text{M}$).



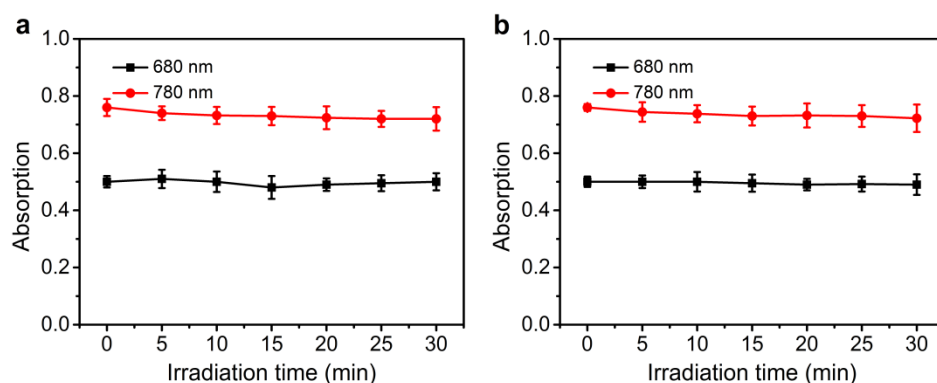
Supporting Figure S5. Proposed mechanism of the model reaction between compound 6 and ClO^- . a) Proposed pathways for the reaction between compound 6 and ClO^- in aqueous environment. b) Matrix assisted laser desorption/ionization time-of-flight (MALDI-TOF) mass spectrum of compound 6 treated with ClO^- .



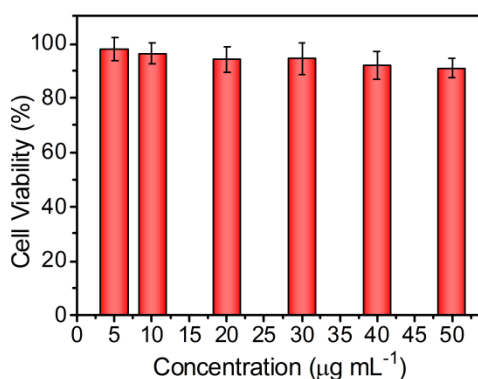
Supporting Figure S6. The influence of pH to the ratiometric absorption (Ab_{780}/Ab_{680}) of the nanoprobe ($30 \mu\text{g mL}^{-1}$) in the absence (black) or presence (red, $11 \mu\text{M}$) of ClO^- .



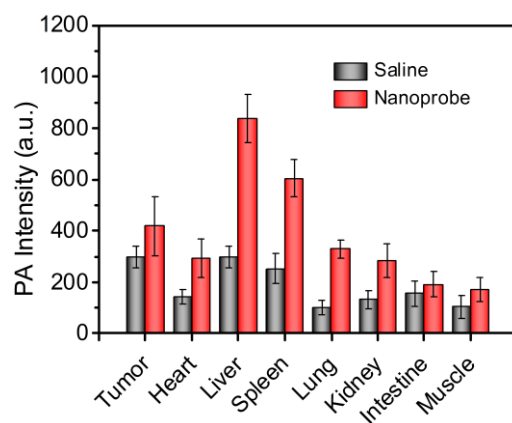
Supporting Figure S7. Comparison of the PA spectra of the SOA before and after NIR775 doping. a) Absorption spectra of the nanoprobe and the SOA (compound 7) in $1\times\text{PBS}$ ($\text{pH} = 7.4$). Their absorbance at 680 nm were adjusted to the same. b) Representative PA spectra of the nanoprobe and the SOA under the same absorbance at 680 nm.



Supporting Figure S8. Absorption stability of the nanoprobe under laser irradiation. a) The absorption fluctuation of the nanoprobe at 680 (black) and 780 nm (red) under 680 nm laser irradiation for 30 min. b) The absorption fluctuation of the nanoprobe at 680 (black) and 780 nm (red) under 780 nm laser irradiation for 30 min. The absorption intensities were simultaneously recorded at 680 and 780 nm. Error bars represent standard deviations of three separate measurements.



Supporting Figure S9. Cytotoxicity studies of the nanoprobe. *In vitro* viability of HeLa cells treated with the nanoprobe solutions at concentrations of 5, 10, 20, 30, 40 and 50 $\mu\text{g mL}^{-1}$ for 24 h. The percentage cell viability of treated cells is calculated relative to that of cells treated with the same volume of PBS (viability was arbitrarily defined as 100%). Error bars represent standard deviations of three separate measurements.



Supporting Figure S10. Ex vivo PA quantification of major organs of mice 24 h after systemic administration of the nanoprobe or saline. The PA data were acquired at 780 nm.